Available online at www.sciencedirect.com
ScienceDirect
Geochimica et Cosmochimica Acta 71 (2007) 3686–3697
Geochimica et Cosmochimica Acta
www.elsevier.com/locate/gca

Experimental study of nickel(II) interaction with calcite: Adsorption and coprecipitation

L.Z. Lakshtanov [a,b,*], S.L.S. Stipp [a]

[a] Department of Chemistry, Copenhagen University, Universitetsparken 5, DK-2100 Copenhagen Ø, Denmark
[b] Institute of Experimental Mineralogy RAS, 142432 Chernogolovka, Russia

Received 12 September 2006; accepted in revised form 10 April 2007; available online 13 April 2007

Abstract

Partitioning of Ni in calcite, $CaCO_3$, was evaluated with the aim of collecting data on partition and distribution coefficients and to enhance understanding about the interaction of Ni with the calcite surface and further incorporation into the bulk. This information will aid in the interpretation of geological processes for safety assessment of waste repositories and contamination of groundwater. Coprecipitation experiments were carried out by the constant addition method at 25 °C and $pCO_2 = 1$ and $10^{-3.5}$ atm. Ni was moderately partitioned from solution into calcite. For dilute solid solutions ($X_{Ni} < 0.001$), Ni partition coefficients were estimated to be ~1 and found to be weakly dependent on calcite precipitation rate in the range of 3–230 nmol m^{-2} s^{-1}. Ni molar fraction in the solid is directly proportional to Ni concentration in the solution. The fit of the data to such a model is good evidence that Ni is taken up as a true solid solution, not simply by physical trapping.

1. INTRODUCTION

Nickel contamination from industrial and mining activities can pose a serious risk to groundwater. Because Ni is toxic to plants and animals, data describing its behaviour and fate are required for valid assessment of risk and designing effective remediation strategies. Because the interaction of calcite with Ni controls its distribution in calcareous environments (Larsen and Postma, 1997), better understanding of the mechanisms responsible for nickel uptake would improve modelling capabilities. Of the two main controlling processes, adsorption and coprecipitation, the latter is more effective on the long term, because trace metals can be ''immobilised'' within the calcite structure, effectively decreasing the chance that they will re-enter the groundwater. On the other hand, Ni accumulation via incorporation can locally increase solid concentration, producing a future Ni source if conditions change and the calcite dissolves.

One example of natural nickel contamination is in groundwater supplies from chalk aquifers in Denmark and south-western Sweden, where trace concentrations of nickel are present as a solid solution in pyrite nodules. As the pyrite is oxidised by draw-down of the water table, Ni is released (Larsen and Postma, 1997). Depending on groundwater conditions, nickel concentrations can vary from barely detectable to a few hundred ppm (~5 μM), well above the Danish legal limit and the World Health Organisation (WHO) recommended value of 20 ppb (0.34 μM). Anthropogenic contamination most commonly arises with industrial operations, where nickel is produced or used in manufacturing. Secondary contamination may result from long term degradation of radioactive waste repositories. ^{59}Ni and ^{63}Ni are produced by neutron activation of ^{58}Ni and ^{62}Ni (both naturally occurring and stable isotopes of nickel) in the structural steels and internal components of nuclear reactor vessels. These radionuclides represent important activation products and will exceed the activity from the other major activation products (Adams et al., 1996). Moreover, the currently most attractive scenario for burial of spent fuel rods is to pack them in stainless-steel canisters. After extended exposure to the decaying waste,

* Corresponding author.
E-mail address: leonidl@geol.ku.dk (L.Z. Lakshtanov).

0016-7037/$ - see front matter © 2007 Elsevier Ltd. All rights reserved.
doi:10.1016/j.gca.2007.04.006

the canisters would become radioactive and corrosion could risk release to the environment.

In recent years, a great deal of information has been gathered about the uptake properties of calcite, especially its propensity for incorporation of divalent cations (Curti, 1999 and references therein). A good deal of information is also available about the uptake behaviour for elements of particular interest for waste repositories (Curti, 1999). In addition to experimental studies that have examined partitioning behaviour between solids and solutions, effective methods have been developed for modelling solid solution formation (Kulik et al., 2000; Curti et al., 2005) and for incorporating parameters to describe solid solution formation in reactive transport equations (Lichtner and Carey, 2006).

Although nickel is toxic as a heavy metal as well as in its radioactive form, surprisingly few experimental studies have been made to define its interaction with soil and sediment minerals in general and only a handful of articles report investigations of Ni interaction with calcite. The only study of Ni adsorption on calcite was published by Zachara et al. (1991). They used a single exchange constant for Ni, as well as for Cd, Mn and Co, to describe sorption over a wide range of pH and Ca activity and surface concentration. The data suggest that Ni, as well as Zn and Co, forms surface complexes that remain hydrated until the cations are incorporated into the bulk structure by recrystallization. In contrast, they propose that Cd and Mn dehydrate soon after their adsorption (Zachara et al., 1991). Hoffmann and Stipp (2001) came to a similar conclusion from their study of the mechanisms of Ni incorporation, using surface sensitive techniques (XPS, TOF-SIMS and AFM). They showed that Ni is included into the calcite structure by rearrangement of the solid, but the uptake is much slower than for Cd or Zn (Stipp et al., 1993; Stipp, 1994). Carlsson and Aalto (1998) studied Ni coprecipitation with calcite using liquid scintillation counting and observed Ni incorporation during recrystallization. They estimated a Ni–calcite partition coefficient of about 2.

The work reported here aimed to investigate calcite's affinity for Ni and to study Ni partitioning into calcite precipitated from electrolyte solutions under strictly controlled conditions. All experimental and solution variables, including calcite precipitation rate, pH, pCO_2, as well as Ca and Ni concentrations were held constant for any given precipitation run. By systematically varying Ni concentration and calcite precipitation rate, the influence of these parameters on Ni partitioning could be determined.

2. THEORETICAL BACKGROUND

2.1. Partition coefficient

Solubility of the Ni–calcite solid solution is described by two equations (Lippmann, 1980), one relating the concentration of $NiCO_3$ in the solid solution with the activities of the Ni^{2+} and CO_3^{2-} ions in the aqueous solution:

$$(Ni^{2+})(CO_3^{2-}) = K^s_{NiCO_3} X_{NiCO_3} f_{NiCO_3} \quad (1)$$

and the other relating the concentration of $CaCO_3$ in the ideal solid solution with the activities of dissolved Ca^{2+} and CO_3^{2-} ions:

$$(Ca^{2+})(CO_3^{2-}) = K^s_{CaCO_3} X_{CaCO_3} f_{CaCO_3}, \quad (2)$$

where $K^s_{NiCO_3}$, $K^s_{CaCO_3}$, f_{NiCO_3}, f_{CaCO_3}, X_{NiCO_3}, and X_{CaCO_3} represent the solubility products, activity coefficients and mole fractions for the $NiCO_3$ and $CaCO_3$ end members.

Dividing Eq. (2) by Eq. (1) and taking into account that for the dilute solid solution $f_{CaCO_3} \to 1$ and $f_{NiCO_3} \to$ const, we have:

$$\frac{X_{NiCO_3}}{X_{CaCO_3}} \frac{(Ca^{2+})}{(Ni^{2+})} = \frac{K^s_{CaCO_3}}{K^s_{NiCO_3} f_{NiCO_3}} = \text{const.} \quad (3)$$

For equally charged cations and dilute solutions ($I < 0.3$), the ratio of the molal scale ion activities in the aqueous phase can be considered to be essentially equal to the ratio of molalities. Under such conditions, Eq. (3) can be rewritten:

$$\frac{X_{NiCO_3}}{X_{Ca}} \frac{m_{Ca^{2+}}}{m_{Ni^{2+}}} = \frac{K^s_{CaCO_3}}{K^s_{NiCO_3} f_{NiCO_3}} = \text{const.} \quad (4)$$

If Ca and Ni complexation are negligible, Eq. (4) coincides with the partition coefficient as defined by Henderson and Kraček (1927):

$$\lambda_{Me} = \frac{X_{Me}}{X_{Ca}} \frac{[Ca]}{[Me]} \quad (5)$$

with the exception that it is the total concentrations of Ca and Me (metal) that are used.

Various models have been developed to predict trace metal partitioning between minerals and aqueous solutions (e.g. Sverjensky, 1984, 1985; Rimstidt et al., 1998; Wang and Xu, 2001). The linear free energy correlation model by Wang and Xu (2001) provides a useful tool to predict an unknown partition coefficient. It takes into account not only the chemical bonding energies of cations within a host mineral but also the excess energies resulting from size differences between the substituting trace ion and the host cations. The Wang and Xu model attempted to predict both the solubility product of $NiCO_{3(s)}$ ($\log K_s = -10.15$) and the Ni partition coefficient in calcite ($\sim$3.5).

It can be seen from Eq. (4) that the partition coefficient is largely influenced by the ratio of solubility product constants of the two pure end member solids. Therefore, knowledge of solubility product values is extremely important for a reliable prediction of a partition coefficient. Some simple and useful correlations to predict partition coefficients are built on utilization of solubility products (Zachara et al., 1991; Curti, 1997, 1999). However, the individual solubility product for nickel-carbonate is not well known. Zachara et al. (1991) noticed the atypical behaviour of Ni in a comparison of surface exchange constants and solubility products of the anhydrous metal carbonates. They suggested that previously reported values for the $NiCO_3$ solubility product, e.g. $\log K_s = -6.34$ (Wagman et al., 1982) and -6.8 (Smith and Martell, 1976) are too high to be reasonable. Grauer (1994) recommended a value for $\log K_s = -11.2 \pm 0.3$ based on extrapolation of

the experimental data of Reiterer (1980). This value falls in the range of data for the solubility of other transition metals.

Among the studies based on correlation that are listed above, Curti (1999) reported partition coefficients for various trace metals in calcite and the solubility of the corresponding carbonates. That work includes not only divalent cations, with their moderate partition coefficients, but also considers monovalent and trivalent metals with very low and extremely high affinity for calcite. Curti (1997) provides two straight line equations derived from linear regression analysis, that correspond to the best fit and a "worst case" scenario (i.e. unfavourable for a radionuclide waste repository). Using the best fit $\log \lambda_{Ni} = -0.784 \log a_{Ni^{2+}} - 4.10$ with $\log K_s = -11.2$ (Grauer, 1994), we obtain $\lambda_{Ni} = 5.8$. With $\log K_s = -10.15$ (Wang and Xu, 2001), we can obtain $\lambda_{Ni} = 0.9$. The same calculations with the "worst" case, $\log \lambda_{Ni} = -0.843 \log a_{Ni^{2+}} - 5.19$, give $\lambda_{Ni} = 1.1$ and 0.1. Thus, these estimates confine the range for a Ni partition coefficient in calcite to something between 0.1 and 6.

Another useful correlation for predicting an unknown partition coefficient is the relationship between selectivity constants, K_{ex}, quantifying sorption, and partition coefficients (Curti, 1999). One expects positive correlation between sorption and incorporation because these processes are tightly interrelated; adsorption is a necessary intermediate step for all incorporation reactions. The correlation between selectivity constants for the sorption of divalent metals on calcite (Zachara et al., 1991) and the corresponding partition coefficient for coprecipitation has a slope very close to unity. This is not surprising because the same chemical factors control the magnitude of both K_{ex} and λ (Zachara et al., 1991). The surface selectivity constant, log K_{ex}, for Ni adsorption onto calcite is 0.51 or $K_{ex} = 3.2$. Thus, one would expect the Ni partition coefficient to be about the same.

2.2. Precipitation rate effect

To obtain the equilibrium partition coefficient, K_D, values required for modeling, the system is assumed to be in equilibrium, that is, the chemical potential of each component is the same everywhere in the system. This assumes that all phases are equilibrated with each other and the spatial distribution of a component is uniform. Partition coefficients determined for natural systems as well as those estimated from experimental data usually differ from equilibrium values because natural environments and experiments rarely reach equilibrium. Thus, distribution of a trace component in the growing crystal is effectively determined by some kinetic process. It is well known (Chernov, 1984) that trace concentration is controlled by the mechanisms of statistical selection in the interfacial region and diffuse relaxation in the bulk crystal and in the surrounding solution. The composition of the adsorption layer is generally different from that in the bulk crystal. If the crystal grows, some ions bound to the surface have to be transferred back to the solution. However, if crystal growth is rapid, adsorbed ions may be trapped and buried in the freshly precipitated material, resulting in solid concentrations that deviate substantially from those predicted by equilibrium partitioning between the crystal and its surroundings. The effectiveness of this entrapment process depends on the interplay between growth rate of the crystal and diffusivity in the boundary layer of the crystal, which determines how efficiently a component can reach the surface by diffusion through the solution. A boundary layer, with a different cation ratio, may be created by decreased concentration at the crystallization surface. In this case, the measured partition coefficient, λ, depends on the precipitation rate, R', as follows (Wang and Xu, 2001):

$$\lambda = \frac{\lambda^0}{1 + (\lambda^0 - 1)R'}. \tag{6}$$

Here, λ^0 represents the equilibrium partition coefficient and $R' = 1 - m^{\infty}_{Ca}/m^{0}_{Ca}$ (where m^{∞}_{Ca} and m^{0}_{Ca} represent Ca concentrations at the crystallization surface and in the bulk solution, respectively) denotes a scaled precipitation rate ranging from 0 to 1. This expression means that the measured partition coefficient approaches 1 with increasing precipitation rate. However, Wang and Xu (2001) stated that numerous experimental data show the partition coefficients for divalent cations in calcite never approach 1, even if they tend in that direction. The activation energy for calcite growth is about 45 kJ mol^{-1} (Nancollas and Reddy, 1971; Takasaki et al., 1994). This suggests that either adsorption onto the surface or incorporation into the crystal lattice is the rate-limiting step. The activation energy for bulk solution diffusion is about 16 kJ mol^{-1} (Nielsen, 1984), so it is unlikely that diffusion in solution would be rate-determining.

Another group of models have been developed to explain the partitioning of trace elements between a solution and a growing crystal (Trainor and Bartlett, 1961; Chernov, 1984; Gilmer, 1984). They account for the effects of increased growth step velocity by means of a decrease in time necessary for trace elements to be selected by an incorporation site. These models are based on the Berthelot–Nernst distribution law (McIntire, 1963):

$$k_D = \frac{C_s}{C_l}, \tag{7}$$

where k_D represents the distribution coefficient and C_s and C_l, the concentrations of the trace component in the solid and the liquid. The distribution coefficient is affected by interplay between solid-state diffusion and precipitation rate as follows (Chernov, 1984):

$$k_D = k^0_D + (k_s - k^0_D) \exp\left(-\frac{D_s}{R \cdot h}\right), \tag{8}$$

where k^0_D represents the equilibrium distribution coefficient, k_s, the distribution coefficient on the growing step of the crystal, D_s, the diffusion coefficient of trace component in the crystal, R, the linear normal growth rate and h, height of the growing step.

It was shown (Dubinina and Lakshtanov, 1997) that Eq. (8) can be expressed in the same way in terms of a partition coefficient:

$$\lambda = \lambda^0 + (\lambda_s - \lambda^0) \cdot \exp\left(-\frac{D_s}{R \cdot h}\right). \quad (9)$$

This equation does not take into consideration the similar diffuse relaxation in the surrounding solution where there is interplay between the crystal growth rate, the transfer of a species from the solution to the surface, and chemical reaction at the surface. During fast crystal growth, the adsorption process is often diffusion controlled and the concentration depends on the distance from the crystal surface. Therefore, at high precipitation rates, a growing crystal may trap species at the ratio of their diffusivities in the bulk solution, which is always nearly 1, and λ tends to 1. When diffusion is not limiting, the solution is able to supply the trace cations to the boundary layer, adsorption is nearly at equilibrium, so at very low precipitation rates, λ approaches its equilibrium value. Between these limiting cases, λ can take values from λ^0 to 1. Depending on the ratio between the equilibrium adsorption and distribution coefficients, λ_s^0 and λ^0, λ may even be an extreme function of the precipitation rate (Dubinina and Lakshtanov, 1997). On the other hand, at low to moderate precipitation rates and when the local conditions within the boundary (or adsorption) layer approach equilibrium, Eq. (9) can be considered as a good approximation. It can be easily seen from this equation that a special case exists when λ_s^0 and λ^0 have similar values. Then, the partition coefficient, λ, is independent of precipitation rate and there is proximity between λ and λ^0 for any value of precipitation rate. This is very similar to the concept of Wang and Xu (2001).

An explicit solution of the growth entrapment problem was presented by Watson and Liang (1995). Their main assumption was that an activity coefficient for a trace element is a function of a spatial variable in the surface layer, a necessary condition for surface enrichment by a trace element. They numerically integrated the mass balance equation to obtain concentration profiles of a surface-enriched element in a growing crystal. Recently, Watson (2004) modified this model to include a depth-dependent diffusivity parameter and possible depletion of some trace elements in the near-surface region. This model does not take into account processes occurring in the surrounding growth solution. According to these models, with increasing precipitation rate, the measured partition coefficient approaches the value inherent for the partition coefficient of the growing step. Since the interface layer is a transition region between aqueous solution and solid phase, one can expect that an "interfacial" partition coefficient is somewhere between the equilibrium partition coefficient and 1.

3. MATERIALS AND METHODS

For coprecipitation experiments, we used reagent grade calcite supplied by Sigma, which had particle diameter on the order of 10 μm. Surface area was about 0.25 m^2/g. The calcite powder was treated to remove the organic inhibitors added during commercial synthesis by washing several times in vessels of fresh, deionised, hot water under CO_2 atmosphere according to the method adopted from Stipp and Hochella (1991).

A method for coprecipitation of Ni-bearing calcite was developed for these experiments by adapting the procedure of Tesoriero and Pankow (1996). It allows the synthesis of solids of a nearly constant composition at a given precipitation rate. For each experiment, 100 ml of $NaClO_4$ solution was held at $T = 25$ °C and $pCO_2 = 1$ atm in a jacketed reaction vessel. Weighed amounts of calcite powder were placed into the reaction vessel to equilibrate the solution with calcite and to provide seed material for precipitation. The powder was held in suspension by an overhead propeller stirrer to prevent grinding of the powder against the bottom of the vessel. To minimize evaporation in long term experiments, the CO_2 gas was first passed through a 0.1 M $NaClO_4$ solution before it was bubbled into the reaction solution.

Precipitation was induced by pumping the two separate solutions, $Ca(ClO_4)_2$ and Na_2CO_3, into the reaction vessel using a peristaltic pump. Molalities of the solutions ranged from 0.025 to 0.425 depending on desirable calcite precipitation rate. Precipitation rate could also be selected by setting the peristaltic pump rate that varied from 0.001 to 0.01 mL/min. Mixing of the solutions caused calcite precipitation; precipitation rate increased until it was equal to the addition rate of Ca and carbonate by the pump. After steady-state precipitation rate was reached, where solution composition in the reaction vessel remained essentially constant (detected by the measurements of Ca concentration as well as pH), a small aliquot (0.1–1 ml) of 7.5×10^{-3} M $Ni(NO_3)_2$ stock solution was added to the initial $Ca(ClO_4)_2$ solution. This resulted in Ni concentration of the feed solutions ranging from 100 to ~6500 ppb. Introduction of the Ni solution had no measurable effect on carbonate alkalinity or pH. Pumping of the solutions continued as before, at the same rate, until a second steady-state condition was reached where Ni concentration remained constant. In some experiments, a Ni aliquot was added to the initial $Ca(ClO_4)_2$ solution from the beginning and we waited for the steady-state condition of constant Ni concentration. The aqueous phase was periodically sampled, filtered through 0.2 μm Sartorius filters, and analyzed for Ca and Ni. Reaching this second steady-state condition is the most important point in the experiment because the Ni molar fraction in the solid at this second steady-state condition can be assumed to be equal to the Ni molar fraction in the feed solution. More correctly, Ni molar fraction, X_{Ni}, in the last precipitate formed at the second steady state can be expressed as follows:

$$X_{Ni} = \frac{[Ni]^0 - [Ni]^{st}}{[Ca]^0 - [Ca]^{st} + [Ni]^0 - [Ni]^{st}}, \quad (10)$$

where $[]^0$ and $[]^{st}$ denote the corresponding molar concentrations in the feed solution and in the reaction vessel at the second steady-state. These calculated values of Ni molar fraction were then used for determining the Ni partition coefficients.

The Ni concentrations of the feed solution were chosen such that the solubility products of pure Ni solid phases (such as $NiCO_{3(s)}$, $Ni(OH)_{2(s)}$) were by no means exceeded, in order to insure that Ni could precipitate as a solid solution and not as a separate, pure Ni phase. Aqueous

speciation calculations for all experiments were performed using PHREEQC (Parkhurst and Appelo, 1999) with the Zachara et al. (1991) constants for Ni speciation included in the database.

At the end of each experiment, the solid phase was rinsed for a few minutes with a calcite-saturated solution, dried at 90 °C for a day and then weighed. Several samples with the highest Ni loadings were checked by X-ray diffraction to ensure that the solid was still only calcite. Calculations with expected intensities for other Ni phases indicate that within a detection limit of about 1%, no crystalline materials other than calcite were found. A part of each solid sample was dissolved in 3.5 M HNO_3 and analyzed for Ni and Ca. Nevertheless, the solid composition values for Ni were not used for determination of λ_{Ni} values obtained using Eq. (4), because of the large uncertainty associated with determining solid composition. Uncertainty arises from errors in estimating overgrowth mass and the composition and its evolution over the course of the pre-steady state period. Ca and Ni concentrations were determined from solution, by atomic absorption spectrometry (AAS) (Perkin–Elmer 5100) with precision better than ±2%.

Ni adsorption experiments were performed at 25 °C with atmospheric CO_2 partial pressure, in calcite equilibrated solutions. The purpose was to establish the role of adsorption on Ni incorporation during calcite growth. At each desired initial concentration, 20 mL of the solution in equilibrium with $CaCO_{3(s)}$ was placed in three 25 mL polyethylene bottles with 1–5 g fresh $CaCO_{3(s)}$ powder. Suspensions were allowed to equilibrate for 24 h. Each bottle was then spiked with 20–200 μL of $NiCl_2$ (22 ppm) solution. The bottles were agitated for 24 h. Samples were taken after 24 h of equilibration, filtered with 0.2 μm Sartorius filters, acidified with HCl and stored for analysis by AAS with flame for Ca concentrations and graphite furnace for Ni.

4. RESULTS

4.1. Adsorption

Nickel sorption on calcite followed the same pattern observed for other divalent cations (McBride, 1979, 1980; Lorens, 1981; Davis et al., 1987; Zachara et al., 1988, 1991; and many others), namely, an initial fast adsorption, followed by slower uptake by coprecipitation or recrystallisation. Recrystallisation is driven by the difference in surface free energy for crystals of different sizes. It can produce a surface coprecipitate when adsorbed ions incorporate into freshly formed surface layers of calcite. In our experiments, steady-state or equilibrium solution concentrations, which were typically reached after 10–15 h, could be used to estimate adsorption. The data, plotted as a Ni isotherm, define a line on a log–log plot (Fig. 1), as was also observed by Zachara et al. (1988, 1991).

In the present study, nickel adsorption was considered to take place through complexation with the calcite surface groups. Surface spectroscopic and microscopic observations have shown that water adsorbs to the calcite surface and this hydrating layer is torn apart by the partially unsatisfied charges associated with Ca and CO_3, resulting in a hydrolysed layer directly in contact with the termination of the calcite bulk structure (Stipp, 1999). The adsorbed water thus becomes OH^- and H^+, sitting respectively over >Ca and $>CO_3$, where the symbol >Ca represents the portion of the $CaCO_3$-surface where Ca atoms on the solid are in contact with solution. OH^-, associated with >Ca, then delocalizes the unsaturated charge on Ca and forms the complex >CaOH. Similarly, H^+ delocalizes the charge on $>CO_3$ and becomes $>CO_3H$ (Stipp and Hochella, 1991; Stipp et al., 1994; Stipp, 1999). Based on these observations, the surface complexation model was developed by Van Cappellen et al. (1993) and extended by Pokrovsky et al. (1999). It assumes that the calcite surface is terminated by two main hydrolysis products, >CaOH and $>CO_3H$.

We can consider Ni adsorption by formation of the surface complex, $>CO_3Ni^+$, by the half-reaction exchange:

$$> CO_3H + Ni^{2+} \Longleftrightarrow > CO_3Ni^+ + H^+ \qquad K_{Ni}. \tag{11}$$

The second half-reaction is that for Ca:

$$> CO_3H + Ca^{2+} \Longleftrightarrow > CO_3Ca^+ + H^+ \qquad K_{Ca}. \tag{12}$$

The overall exchange reaction is

$$> CO_3Ca^+ + Ni^{2+} \Longleftrightarrow > CO_3Ni^+ + Ca^{2+} \qquad K_{ex} \tag{13}$$

where the surface selectivity constant is defined:

$$K_{ex} = \frac{[Ca^{2+}]}{[Ni^{2+}]}\left(\frac{[> CO_3Ni^+]}{[> CO_3Ca^+]}\right)^n, \tag{14}$$

and where $[Ca^{2+}]$ and $[Ni^{2+}]$ represent the free ion solution concentrations and $[>CO_3Ni^+]$ and $[>CO_3Ca^+]$, the total adsorbed concentrations. If $n = 1$, as is the case for Ni and all other divalent metals except Zn (Zachara et al., 1991), K_{ex} is formally equivalent to the partition coefficient Eq. (5). Eqs. (11) and (12) allow us write:

$$\log K_{ex} = \log K_{Ni} - \log K_{Ca}. \tag{15}$$

Stability constants were optimized using the non-linear least-squares optimization program, FITEQL Version 3.2 (Herbelin and Westall, 1996). The input of experimental adsorption data into FITEQL was made as described in (Herbelin and Westall, 1996) using a dummy component Ni_{ad}. This dummy component was the derived adsorbed Ni concentration, which we found from the difference between the total added Ni and the Ni concentration we analysed in the solution (Table 2).

Calcite surface site density was estimated from the atomic spacing of the surface unit cell. On the $\{10\bar{1}4\}$ plane, which is the surface that is most commonly observed on commercially available calcite powder used in uptake experiments, the surface unit cell is 4.99 Å wide and 8.10 Å long. It includes two Ca and two CO_3 groups per 40.42 $Å^2$. Thus, calcite has about 5×10^{-18} sites/m^2 or 8.22 μmol sites/m^2 for a cation or an anion.

In modeling, we chose either the Electrical Double Layer (EDL) Constant Capacitance Model (CCM) or no electrostatic model. CCM was used to compare our results with those of Pokrovsky et al. (2002) who modeled the experimental data of Zachara et al. (1991) for divalent metal adsorption onto calcite. The complexation reactions rele-

Table 1
Complexation reactions relevant to the calcite–CO_2–Ni^{2+}–Ca^{2+}–H^+ system at 25 °C and $I = 0$, used in the FITEQL model. Data were compiled from Zachara et al. (1991), Van Cappellen et al. (1993) and Pokrovsky et al. (1999)

Equilibrium reaction	$\log K$
$H_2O = H^+ + OH^-$	−14
$Ca^{2+} + H_2CO_3 = CaHCO_3^+ + H^+$	−5.4
$Ca^{2+} + H_2O = CaOH^+ + H^+$	−12.6
$Ca^{2+} + H_2CO_3 = CaCO_3^0 + 2H^+$	−13.55
$H_2CO_3 = CO_3^{2-} + 2H^+$	−16.7
$H_2CO_3 = HCO_3^- + H^+$	−6.4
$Ni^{2+} + H_2CO_3 = NiCO_3^0 + 2H^+$	−12.5
$Ni^{2+} + H_2CO_3 = NiHCO_3^+ + H^+$	−4.18
$Ni^{2+} + H_2O = NiOH^+ + H^+$	−9.86
$Ni^{2+} + H_2O = Ni(OH)_2^0 + 2H^+$	−19
$> CO_3H => CO_3^- + H^+$	−5.1
$>CO_3H + Ca^{2+} = >CO_3Ca^+ + H^+$	−1.7
$> CaOH + H^+ => CaOH_2^+$	11.5
$>CaOH + H_2O = >CaO^- + H^+$	−12
$>CaOH + H_2CO_3 = >CaHCO_3 + H_2O$	6.8
$> CaOH + H_2CO_3 => CaCO_3^- + H^+ + H_2O$	0.4

vant to the calcite surface–CO_2–Ni^{2+}–Ca^{2+}–H^+ system, used in the model, are summarized in Table 1. We did not vary the value of capacitance of the double layer (κ) but rather, we fixed it at 15 F/m^2 as calculated using the formula $\kappa = I^{1/2}/\alpha$, where α is an empirical parameter equal to 0.006 for calcite (Pokrovsky et al., 2002). The optimization procedure led to a $\log K_{Ni}$ value of -1.15 ± 0.05, which is somewhat lower than $\log K_{Ni} = -0.95$ obtained by Pokrovsky et al. (2002).

Almost the same value of $\log K_{Ni} = -1.18 \pm 0.05$ was obtained using the non-electrostatic model. This is not surprising because of the strong relationship between surface charge and electrostatic potential which is typical for carbonates (high capacity of the electrical double layer). Moreover, electrostatics plays an insignificant role because the overall process of exchange of two equivalent cations, Ni^{2+} and Ca^{2+}, proceeds without surface charging.

From Eq. (15), a surface selectivity constant can be found to be $\log K_{ex} = -1.18 + 1.7 = 0.52$. This value is in excellent agreement with $\log K_{ex} = 0.51$ obtained by Zachara et al. (1991).

4.2. Coprecipitation

A first steady-state condition, where calcite precipitation rate was constant, was typically reached within 25–30 h after beginning a run, depending on initial $Ca(ClO_4)_2$ concentration. After the aliquot of $Ni(NO_3)_2$ stock solution was added, Ni concentration in the reaction solution increased and a second steady-state condition with constant Ni concentration was attained within 3–5 days, depending on Ca and Ni initial concentrations. The experimental conditions, including aqueous and solid composition and calcite precipitation rate, are listed in Table 3.

The Ni partition coefficients were calculated using Ca^{2+} and Ni^{2+} concentrations Eq. (4). For the runs with $pCO_2 = 1$ atm, where pH is about 6, total dissolved metal concentration is essentially the same as free ion concentration, so there was no difference whether Eq. (4) or Eq. (5) was used. In contrast, when $pCO_2 = 10^{-3.5}$ atm where pH is about 8.3, $NiCO_3^0$ concentration is a significant part of the total dissolved Ni present. For this reason, the Ni partition coefficients for runs with $pCO_2 = 10^{-3.5}$ atm were derived from both Eqs. (4) and (5). Ni^{2+} concentrations were determined using PHREEQC (Parkhurst and Appelo, 1999), for Ni speciation (Zachara et al., 1991) and $\log K$ for $NiCO_3^0 = 4.2$ as reported by Baeyens et al. (2003).

One can see in Table 3, that Ni molar fraction in the solid, determined using Ni and Ca aqueous concentrations in the feed solution, is sometimes slightly higher than that obtained using concentration from the calcite overgrowths. This occurs because the composition of the solid is not uniform. In addition to the mass contributed by the original seed crystals and their overgrowths precipitated during attainment of the first steady-state, which are free of Ni and therefore easy to account for, the total mass of the final material also contains Ni-bearing overgrowths formed during the period where the system was attempting to reach its second steady-state condition. From the moment when Ni was first added to the $Ca(ClO_4)_2$ feed solution, until the attainment of the second steady-state condition, Ni concentration in the solution was not constant, so its incorporation into calcite varied. Therefore, for the calculation of the Ni–calcite partition coefficients, we used only the values of Ni molar fraction calculated from the solution concentration data; the molar fraction of $NiCO_3$ in the solid was assumed to be x for the $Ni_xCa_{1-x}CO_3$ feed solution. In some runs (#16, 27, 28), the overgrowth mass was too small to allow determination of Ni with sufficient accuracy to be useful. Concentrations determined from the solids have not been used for any of the calculations.

The experiments were designed to investigate Ni incorporation in calcite for precipitation rates ranging from 3 to about 230 nmol/m^2 s, where m^2 refers to the surface area of seed material. As seen in Fig. 2, for the whole range of the precipitation rate, λ decreases with R. The best fit line drawn through the data for $pCO_2 = 1$ atm, yields the following relationship:

Table 2
Ni concentrations for the adsorption experiments: $pCO_2 = 10^{-3.5}$ atm; pH ~ 8.3; $[Ca]_{eq} = 5 \times 10^{-4}$ M; $I \sim 0.001$; each $[Ni]_{eq}$ value is averaged over three parallel runs

Run #	$[Ni]_{tot}$, 10^{-6} M	$[Ni]_{eq}$, 10^{-6} M	$[Ni]_{ad}$, 10^{-7} M
1	0.75	0.69	0.6
2	1.49	1.38	1.1
3	1.49	1.39	1.0
4	2.02	1.85	1.7
5	2.24	2.07	1.7
6	2.98	2.74	2.4
7	2.98	2.76	2.2
8	2.98	2.77	2.1
9	3.52	3.25	2.7
10	3.73	3.44	2.9
11	3.73	3.45	2.8

$$\log \lambda = -0.04 \log R + 0.02, \quad (16)$$

where R represents precipitation rate in nmol/m^2 s.

Fig. 3 shows X_{NiCO3} for calcite precipitated at all rates as a function of the steady-state $[Ni^{2+}]/[Ca^{2+}]$ ratio in the solution at $pCO_2 = 1$ and $10^{-3.5}$ atm. All the data correlate linearly along the line with zero intercept and slope equal to λ. Such dependence is the reason why the Ni partition coefficient, λ, is independent of both X_{Ni} and $[Ni^{2+}]$ (not shown here). The Ni partition coefficients determined for the single data points ranged from 0.93 to 1.15, with an average value of 1.09.

5. DISCUSSION

The experiments described here illustrate the relationship between calcite precipitation rate and Ni partitioning. Compared to other di- and trivalent cations (Lorens, 1981; Tesoriero and Pankow, 1996), the Ni partition coefficient is only very weakly dependent on precipitation rate. From Eq. (16), one can see that for Ni, $d\lambda/dR = -0.042$, whereas for Sr, it is about 0.25, for Mn, 0.27, and for Cd, −0.19 (Lorens, 1981). Such difference is consistent, because the mineral-water interface is a

Table 3
Experimental conditions for coprecipitation runs

N	$[Ca]^0$, ppm	$[Ca]^{st}$ ppm	$[Ni]^0$ ppb	$[Ni]^{st}$ ppb	Ionic strength, mol/L	pH	Run duration[a], min	R, nmol/m^2 s	X_{Ni}[b]	X_{Ni}[c]	λ[d]
1	3910	413	110	11	0.19	6.10	18980	16	1.92e-5	1.9e-5	1.06
2	3910	425	160	16	0.19	6.09	18980	12	2.80e-5	2.5e-5	1.10
3	3905	416	300	29	0.19	6.13	18980	9	5.27e-5	4.9e-5	1.11
4	3900	376	410	37	0.19	6.16	18980	11	7.18e-5	7.0e-5	1.08
5	3900	350	530	45	0.19	6.18	18980	11	9.26e-5	9.2e-5	1.06
6	3890	346	1120	93	0.19	6.19	18980	14	1.96e-4	1.7e-4	1.08
7	6900	780	185	20	0.34	5.96	10000	75	1.83e-5	1.5e-5	1.05
8	6900	780	398	44	0.34	5.95	10000	77	3.92e-5	3.6e-5	1.03
9	6890	742	833	89	0.34	5.99	10000	85	8.20e-5	8.1e-5	1.01
10	6900	676	1059	101	0.34	6.01	10000	84	1.04e-4	1.0e-4	1.03
11	6880	661	1435	136	0.34	6.02	10000	91	1.42e-4	1.4e-4	1.02
12	6880	653	1604	155	0.34	6.01	10000	98	1.92e-4	1.4e-4	0.98
13	8310	310	135	5	0.42	6.15	9540	107	1.10e-5	1.0e-5	1.01
14	8310	312	329	12	0.42	6.14	9540	96	2.69e-5	2.3e-5	1.03
15	8310	288	638	23	0.42	6.18	9540	100	5.21e-5	5.0e-5	0.93
16	8300	237	1015	29	0.42	6.23	9540	86	8.29e-5	—	1.00
17	8297	230	1583	46	0.42	6.24	9540	111	1.29e-4	1.2e-4	0.95
18	8295	253	1714	52	0.42	6.19	9540	107	1.40e-4	1.4e-4	1.01
19	4502	480	150	15	0.20	6.06	15540	15	2.28e-5	2.3e-5	1.07
20	4500	480	201	21	0.20	6.05	15540	13	3.04e-5	2.9e-5	1.05
21	4480	425	339	29	0.20	6.08	15540	17	5.18e-5	5.2e-5	1.12
22	4480	420	858	75	0.20	6.08	15540	16	1.31e-4	1.3e-4	1.08
23	4470	420	1545	135	0.20	6.08	15540	16	2.59e-4	2.6e-4	1.08
24	4467	425	2005	168	0.20	6.08	15540	17	3.08e-4	3.1e-4	1.15
25	4465	430	3266	296	0.20	6.09	13300	15	5.0e-4	5.1e-4	1.07
26	4465	425	3654	319	0.20	6.09	13300	15	5.6e-4	5.5e-4	1.10
27	16820	227	304	4	0.84	6.18	8460	231	1.21e-5	—	1.01
28	16820	473	203	6	0.84	6.03	8460	221	8.40e-6	—	0.95
29	16810	367	838	19	0.84	6.15	8460	231	3.38e-5	3.2e-5	0.96
30	16800	294	1656	29	0.84	6.16	8460	232	6.68e-5	6.4e-5	1.00
31	16800	432	3402	92	0.84	6.08	8460	214	1.37e-4	1.2e-4	0.94
32	16770	275	6637	110	0.64	6.20	8460	222	2.68e-4	2.4e-4	0.99
33	3990	480	434	49	0.19	6.08	9960	37	7.44e-5	7.4e-5	1.07
34	3990	504	773	91	0.19	6.07	9960	34	1.33e-4	1.2e-4	1.08
35	3990	494	1182	148	0.19	6.10	9960	32	2.20e-4	2.2e-4	1.08
36	3990	470	434	45	0.19	6.09	48960	3	7.49e-5	7.5e-5	1.15
37	3990	422	773	70	0.19	6.10	48960	3	1.34e-4	1.3e-4	1.19
38	3990	389	1182	99	0.19	6.12	48960	3	2.04e-4	2.0e-4	1.18
39	1235	35	519	15	0.06	8.36	8640	21	2.85e-4	2.7e-4	1.12 (0.98)
40	1235	37	985	31	0.06	8.35	8640	23	5.40e-4	5.3e-4	1.09 (0.95)
41	2510	39	2019	33	0.13	8.30	8640	37	5.45e-4	5.2e-4	1.09 (0.95)
42	2510	32	2088	28	0.13	8.34	8640	38	5.64e-4	5.4e-4	1.09 (0.95)
43	3320	40	3254	40	0.17	8.40	8640	37	6.64e-4	6.3e-4	1.12 (0.98)
44	3320	37	1519	18	0.17	8.35	8640	37	3.10e-4	3.0e-4	1.08 (0.94)

[a] time from the moment of Ni addition to the end of the run.
[b] Calculated from the solution concentration data using Eq. (10).
[c] Obtained from the solid concentration data.
[d] Determined with Eq. (4) (values in the brackets are calculated using Eq. (5)).

transition region between the solution and the solid phase. So for elements with $\lambda^0 > 1$, it can be expected that

$$\lambda^0 > \lambda_s > 1 \tag{17}$$

and for the elements with $\lambda^0 < 1$,

$$\lambda^0 < \lambda_s < 1 \tag{18}$$

where λ_s represents the partition coefficient for the interfacial layer. Whichever limiting stage of partitioning we consider: (i) diffusion in the surrounding solution or (ii) in the interfacial region of the solid, the closer λ^0 is to λ_s or 1, the weaker is the rate dependence of the partition coefficient. It is easy to see from Eqs. (6) and (9) that $d\lambda/dR'$ is proportional to either $(\lambda_s - \lambda^0)$ or $(1 - \lambda^0)$.

Differentiation of Eq. (6) gives

$$\frac{d\lambda}{dR'} = -\frac{\lambda^0(\lambda^0 - 1)}{1 + 2R'(\lambda^0 - 1) + R'^2(\lambda^0 - 1)^2} \tag{19}$$

when $\lambda^0 \ll 1$ (which is the case for Sr and Ba), Eq. (19) can be simplified to

$$\frac{d\lambda}{dR'} \approx \frac{\lambda^0}{(1 - R')^2}. \tag{20}$$

From this equation, it follows that at high precipitation rates, $d\lambda/dR'$ tends to very high values, whereas during slow precipitation, $d\lambda/dR'$ approaches λ^0:

$$\frac{d\lambda}{dR'} \approx \lambda^0. \tag{21}$$

This is exactly what happens for partitioning of Sr and Ba: $d\lambda/dR'$ is very high while precipitation is rapid and it levels off as precipitation rate decreases (e.g. Tesoriero and Pankow, 1996, Figs. 2 and 4). In the case where $\lambda^0 \gg 1$, Eq. (19) reduces to

$$\frac{d\lambda}{dR'} \approx -\frac{(\lambda^0)^2}{(1 + R'\lambda^0)^2} \tag{22}$$

and the opposite behaviour is observed. At high R, $d\lambda/dR'$ levels off and approaches –1 but the partition coefficient changes most in the range where precipitation rates are slowest. At low precipitation rates

$$\frac{d\lambda}{dR'} \approx -(\lambda^0)^2. \tag{23}$$

Therefore, the higher the λ^0, the more rapid λ increases with decreasing R. Thus, for very low precipitation rates, completely different behaviour should be observed for the elements with $\lambda^0 < 1$ (such as Sr, Ba, Na, Cs) and $\lambda^0 > 1$ (such as Cd, Mn, Co). Comparison of Eqs. (21) and (23) shows that λ changes much faster if $\lambda^0 > 1$ than if $\lambda^0 < 1$. This important feature was also demonstrated by Watson (2004) in the special case when ion diffusivity varies with proximity to the crystal surface.

For Ni, the partition coefficient is predicted to be slightly higher than 1 (this paper, Introduction; also Wang and Xu, 2001; Curti, 1999) and this correlates with results from experiments on calcite recrystallisation (Carlsson and Aalto, 1998). From Eq. (17), the partition coefficient in the interfacial region is likely close to 1. Thus, the Ni partition coefficient very loosely depends on calcite precipitation rate, because its range is constrained by λ^0 and 1 (or λ_s).

It should be noted that for Sr and Ba, i.e., the elements with $\lambda^0 < 1$, the dependence of partition coefficient on calcite precipitation rate leveled off as precipitation rate decreased to $R < 30$–40 nmol/min mg (Lorens, 1981; Tesoriero and Pankow, 1996). In contrast, for elements with $\lambda^0 > 1$, i.e., Cd, Mn, Co, partition coefficient changed linearly (in log–log scale) over the entire range of precipitation rate, from rapid, to the extremely slow region which represents calcite recrystallization (Lorens, 1981; Tesoriero and Pankow, 1996). The behaviour of Ni reflects this. On Fig. 1, $\log\lambda$ increases linearly with decreasing precipitation rate, to its very low values of about 3 nmol/m^2 s. This rate approaches the upper limit for recrystallization rates found in the literature (Lorens, 1981; Davis et al., 1987; Tesoriero and Pankow, 1996; Curti et al., 2005), which range from 7×10^{-3} to 3 nmol/m^2 s. However, the precipitation rates adopted in the present work are much lower than either the rate of recrystallization of aragonite to calcite (Lorens, 1981), which is about 400 nmol/m^2 s, or the precipitation rate of biogenic calcite, which is 7000–27,000 nmol/m^2 s (Lorens, 1981).

Extrapolation of our experimental data to a lower limit ($\sim 10^{-2}$ nmol/m^2 s) using Eq. (16) gives λ of about 1.5. It is likely that this value is not exceeded in any natural or laboratory calcite (re)crystallization so the Ni partition coefficient probably always falls within the limits of 1–1.5. Nevertheless, the true equilibrium value for the Ni partition coefficient still remains unknown. The theoretical models and empirical correlations (Wang and Xu, 2001; Curti, 1999) predict it to be about 3, which is consistent with the surface selectivity constant, $K_{ex} = 3.0$, measured in this work, and $K_{ex} = 3.2$ obtained by Zachara et al. (1991).

The dependence of partition coefficient on precipitation rate is so low that the Ni molar fraction incorporated by calcite as a function of $[Ni^{2+}]/[Ca^{2+}]$ in the solution is reasonably approximated by a single straight line (Fig. 3). Inspection of Eq. (4) shows that $[Ni^{2+}]/[Ca^{2+}]$ is expected to be proportional to Ni molar fraction in the solid phase, X_{Ni}, which is demonstrated by the experimental data. This is the main evidence that Ni is incorporated by the formation of a solid solution. Moreover, Figs. 2 and 3 show that data obtained at different pCO_2 (1 and $10^{-3.5}$ atm) are governed by the same dependencies. This verifies that a change in pCO_2 does not result in a change in the Ni incorporation mechanism in spite of an implied effect on calcite surface speciation by CO_2 partial pressure changes (Pokrovsky et al., 1999). While surface selectivity constants for divalent metals clearly correlate with partition coefficients (Curti, 1999), interrelation between adsorption and incorporation is not so obvious. For example, at $pCO_2 = 1$ atm (pH $\sim$ 6), Ni adsorption on calcite is not measurable whereas Ni incorporation is significant.

Partition coefficients measured in the present work ($\lambda \sim 1$) indicate that Ni incorporation into calcite is expected to be moderate, in contrast with incorporation of trivalent and tetravalent lanthanides and actinides, which are expected to incorporate strongly ($\lambda \sim 20$–1000)

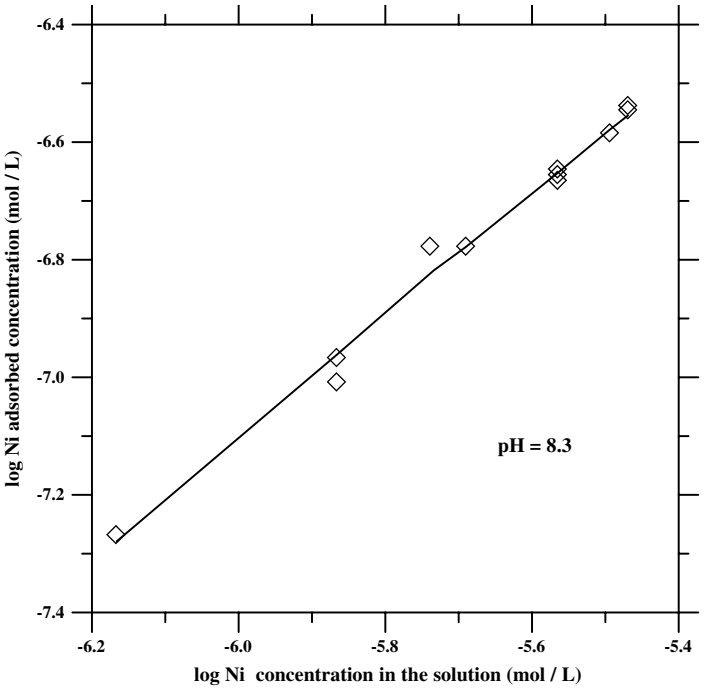

Fig. 1. Sorption isotherm of Ni on calcite at $pCO_2 = 10^{-3.5}$ atm (pH ~ 8.3); symbols, experimental data; line, FITEQL model. Every point was averaged over three parallel runs.

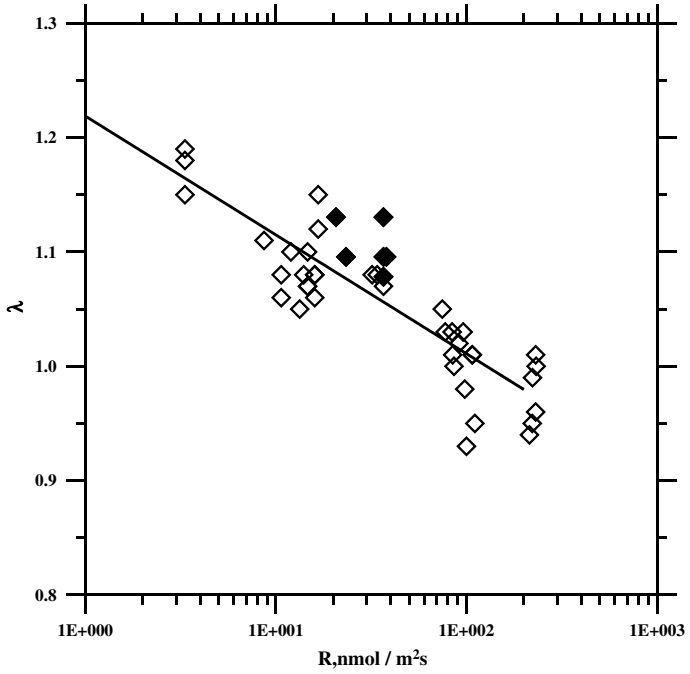

Fig. 2. Ni partition coefficient, λ, plotted as a function of calcite precipitation rate, R. Open symbols denote λ obtained at $pCO_2 = 1$ atm; closed symbols, λ at $pCO_2 = 10^{-3.5}$ atm determined with $\log K_{NiCO3(aq)} = 4.2$.

whereas incorporation of elements such as Na, Sr, Ba, Cs would be weak ($\lambda < 1$).

Let us now evaluate the effects of Ni coprecipitation with calcite using the model developed by Curti (1997), which was intended to describe a closed system representing low and intermediate level radioactive waste (L/ILW) repositories. This model allows estimation of the dissolved, adsorbed and coprecipitated fractions of the trace element inventory during degradation of cement phases and formation of secondary calcite from the resulting high pH, high

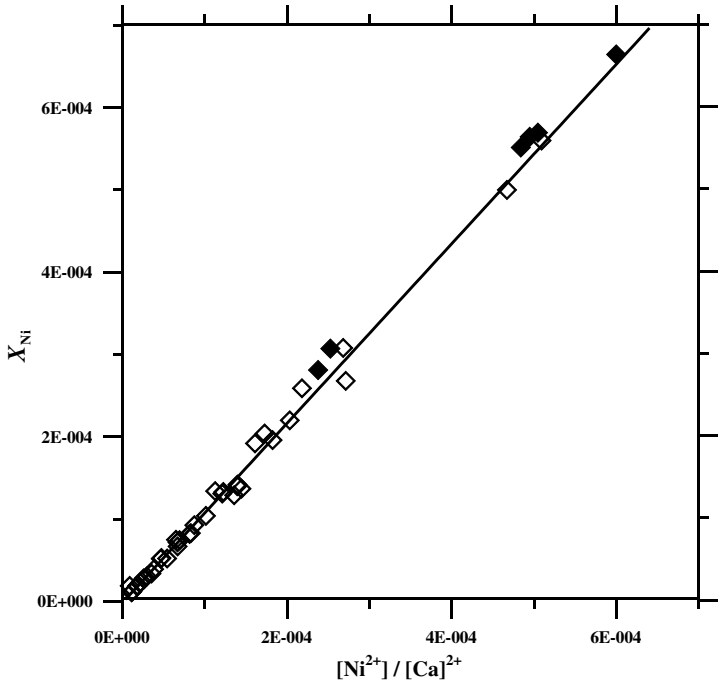

Fig. 3. Ni molar fraction in the solid, X_{Ni}, as a function of the steady state Ni^{2+} to Ca^{2+} concentration ratio in the solution $[Ni^{2+}]/[Ca^{2+}]$. Open symbols represent results obtained for experiments where $pCO_2 = 1$ atm; closed symbols, Ni^{2+} at $pCO_2 = 10^{-3.5}$ atm determined with $\log K_{NiCO3(aq)} = 4.2$.

Ca activity solutions. The coprecipitated fraction (Curti, 1997) of the element inventory is expressed as:

$$x_c = 1 - \exp\left(\frac{\lambda n}{V_p R[C_f]}\right),$$

where n represents the total amount of Ca in the system; V_p, the water-filled pore volume; $[C_f]$, the concentration of Ca in the pore water; R, the retention factor

$$R = 1 + K_d \frac{\rho(1-\varepsilon)}{\varepsilon},$$

K_d, the distribution coefficient for sorption of the element on calcite; ρ, the density of the solid phase (pores excluded) and ε, its porosity. The parameter values used for the model calculations refer to the L/ILW repository at Wellenberg, Switzerland (Curti, 1999) and are as follows: $\rho = 2600\ kg\ m^{-3}$; $\varepsilon = 0.13$; $V_p = 5.4 \times 10^4\ m^3$; $n = 1.15 \times 10^9$ mol; $[C_f] = 8.1\ mol\ m^{-3}$. We have adopted the distribution and partition coefficients from the present work: $K_d = 0.005\ m^3\ kg^{-1}$ and $\lambda = 1.5$. The model calculates that initially, almost the entire Ni inventory is adsorbed. After only 1% of the initial dissolved Ca is converted to calcite, 77% of Ni has coprecipitated. When 2% of Ca is precipitated as calcite, almost the entire Ni pool (95%) has been fixed in the solid phase. Thus, coprecipitation of Ni with calcite is an effective mechanism for reducing Ni mobility in natural systems.

6. CONCLUSIONS

The interactions of Ni with calcite (adsorption and coprecipitation) were investigated in $NaClO_4$ solutions at 25 °C and $pCO_2 = 1$ and $10^{-3.5}$ atm. Coprecipitation experiments maintained constant composition in the aqueous phase, allowing synthesis of solids with a nearly constant composition at a given precipitation rate. From the results, we conclude:

1. Dissolved Ni is moderately partitioned into calcite. For dilute solid solutions ($X_{Ni} < 0.001$), Ni partition coefficients are estimated to be slightly higher than 1.
2. Ni followed the behaviour of other elements with $\lambda^0 > 1$ (Cd, Mn, Co) for which equilibrium λ^0 values are never achieved. The Ni partition coefficient depends only weakly on the calcite precipitation rate over the entire range examined (3–230 nmol $m^{-2}\ s^{-1}$). The very weak dependence on precipitation rate could be explained by the proximity of the Ni equilibrium partition coefficient λ^0 to 1.
3. Extrapolation of our experimental results to lower recrystallization rates ($\sim 10^{-2}$ nmol/m^2 s) gives a λ value of about 1.5. It may be that this value is never exceeded in any natural or laboratory calcite (re)crystallization process so the Ni partition coefficient may always lie within the limits of 1–1.5. Nevertheless, the true equilibrium value of Ni partition coefficient is still not known. It may be about 3, as predicted by some theoretical models and empirical correlations (Wang and Xu, 2001; Curti, 1999). This is consistent with the surface exchange constant, $K_{ex} = 3.0$, measured in this study and $K_{ex} = 3.2$, obtained by Zachara et al. (1991).
4. Ni molar fraction in the solid is directly proportional to Ni concentration in the solution. The fit of the data to such a model is good evidence that Ni is taken up as a true solid solution, not simply by physical trapping.

5. Results of the model calculations show that coprecipitation of Ni with calcite is likely to be an effective mechanism for reducing Ni mobility in natural groundwater systems.

ACKNOWLEDGMENTS

We thank Vagn Moser and Malene Dolberg for technical support and Lone Karlby for the preliminary experiments. This work grew out of a project intended to decrease nickel release to groundwater from chalk aquifers in Roskilde Amt, Denmark, and was encouraged by participation in the FUNMIG project under the 6. Framework EURATOM program, but it was completely funded by the Danish Natural Sciences Research Council (FNU) through Grant 21-04-0538. The manuscript was improved by comments from Associate Editor Jacques Schott and three anonymous reviewers.

REFERENCES

Adams, J. P., Carboneau, M. L. and Allred, W. E. (1996) Selected radionuclides important to low-level radioactive waste management, DOE/LLW-238. Idaho National Engineering and Environmental Laboratory, Idaho Falls, Idaho, USA.

Baeyens B., Bradbury M. H. and Hummel W. (2003) Determination of aqueous nickel-carbonate and nickel-oxalate complexation constants. *J. Sol. Chem.* **32**, 319.

Carlsson, T. and Aalto, H. (1998) Coprecipitation of Ni with calcite: an experimental study. In *Scientific Basis for Nuclear Waste Management XXI*, (eds. Ch. McCombie and I. G. McKinley). Mat. Res. Soc. Symp. Proc. 506, 621–627.

Chernov A. A. (1984) *Modern Crystallography III: Crystal Growth*. Springer, Berlin.

Curti, E. (1997) Coprecipitation of radionuclides: basic concepts, literature review and first applications. PSI-Report 97-10, Paul Scherrer Institut, Villigen.

Curti E. (1999) Coprecipitation of radionuclides with calcite: estimation of partition coefficients based on review of laboratory investigations and geochemical data. *Appl. Geochem.* **14**, 433–445.

Curti E., Kulik D. A. and Tits J. (2005) Solid solutions of trace Eu(III) in calcite: thermodynamic evaluation of experimental data over a wide range of pH and pCO_2. *Geochim. Cosmochim. Acta* **69**, 1721–1737.

Davis J. A., Fuller C. C. and Cook A. D. (1987) A model for trace metal sorption processes at the calcite surface: adsorption of Cd^{2+} and subsequent solid solution formation. *Geochim. Cosmochim. Acta* **51**, 1477–1490.

Dubinina, E. O. and Lakshtanov, L. Z. (1997) Separation of the oxygen isotopes while the synthesis of quartz under hydrothermal conditions. *Proc. Rus. Min. Soc. CXXVI*, N6, 11–22 (in Russian).

Gilmer G. H. (1984) Models of impurity trapping during rapid solidification. *Mater. Sci. Eng.* **65**, 15–25.

Grauer, R. (1994) Vereinigte Löslichkeitsprodukte von M(II)-Schwermetallkarbonaten. Technical Report TM-44-94-05. Paul Scherrer Institute, Villigen, Switzerland.

Henderson L. M. and Kraček F. C. (1927) The fractional precipitation of barium and radium chromates. *J. Am. Chem. Soc.* **49**, 739–749.

Herbelin A. L. and Westall J. C. (1996) FITEQL: A Computer Program for Determination of Chemical Equilibrium Constants from Experimental Data. Version 3.1. Report 94-01. Department of Chemistry, Oregon State University, Corvallis, OR, USA.

Hoffmann and Stipp S. L. S. (2001) The behavior of Ni^{2+} on calcite surfaces. *Geochim. Cosmochim. Acta* **65**, 4131–4139.

Kulik D. A., Kersten M., Heiser U. and Neumann T. (2000) Application of Gibbs energy minimization to model early-diagenetic solid-solution aqueous-solution equilibria involving authigenic rhodochrosites in anoxic Baltic Sea sediments. *Aqua. Geochem.* **6**, 147–199.

Larsen F. and Postma D. (1997) Nickel mobilization in a groundwater well field: release by pyrite oxidation and desorption from manganese oxides. *Environ. Sci. Technol.* **31**, 2589–2595.

Lichtner P. C. and Carey J. W. (2006) Incorporating solid solutions in reactive transport equations using a kinetic discrete-composition approach. *Geochim. Cosmochim. Acta* **70**, 1356–1378.

Lippmann F. (1980) Phase diagrams depicting aqueous solubility of binary mineral systems. *Neues Jahrb. Miner. Abh.* **139**, 1–25.

Lorens R. (1981) Sr, Cd, Mn, and Co distribution coefficients in calcite as a function of calcite precipitation rate. *Geochim. Cosmochim. Acta* **45**, 553–561.

McBride M. B. (1979) Chemisorption and precipitation of Mn^{2+} at $CaCO_3$ surfaces. *Soil. Sci. Soc. Am. J.* **41**, 693–698.

McBride M. B. (1980) Chemisorption and precipitation of Cd^{2+} on calcite surfaces. *Soil. Sci. Soc. Am. J.* **44**, 26–28.

McIntire W. L. (1963) Trace elements partition coefficients—a review of theory and application to geology. *Geochim. Cosmochim. Acta* **27**, 1209–1264.

Nancollas G. H. and Reddy M. M. (1971) The crystallization of calcium carbonate. II. Calcite growth mechanism. *J. Colloid Interface Sci.* **37**, 824–830.

Nielsen A. E. (1984) Electrolyte crystal growth mechanisms. *J. Crystal Growth* **67**, 289–310.

Parkhurst, D. L. and Appelo, C. A. J. (1999) User's guide to PHREEQC (Version 2)—A computer program for speciation, bath-reaction, one-dimensional transport, and inverse geochemical calculations. *Water-Resources Investigations Report 99-4259*. USGS, Denver CO, USA.

Pokrovsky O. S., Schott J. and Thomas F. (1999) Dolomite surface speciation and reactivity in aquatic systems. *Geochim. Cosmochim. Acta* **63**, 3133–3143.

Pokrovsky O. S., Schott J. and Mielczarski J. A. (2002) Surface speciation of dolomite and calcite in aqueous solutions. In *Encyclopedia of Surface and Colloid Science*, (ed. A. Hubbard), pp. 5081–5095. Marcel Dekker, Inc., New York.

Reiterer F. (1980) Loslichkeitskonstanten und Freie Bildungsenthalpien neutraler Ubergangsmetallcarbonate, $MnCO_3$, $FeCO_3$, $CoCO_3$, $NiCO_3$, $CuCO_3$, $ZnCO_3$. PhD Thesis, Montanuniversitat, Leoben, Austria.

Rimstidt J. D., Balog A. and Webb J. (1998) Distribution of trace elements between carbonate minerals and aqueous solutions. *Geochim. Cosmochim. Acta* **62**, 1851–1863.

Smith, R. M. and Martell, A. E. (1976) Critical stability constants. Inorganic complexes, vol. 4, Plenum Press, New York.

Stipp S. L. S. (1994) Understanding interface processes and their role in the mobility of contaminants in the geosphere: the use of surface sensitive techniques. *Eclogae Geol. Helvetia* **87**, 335–355.

Stipp S. L. S. (1999) Toward a conceptual model of the calcite surface: hydration, hydrolysis and surface potential. *Geochimica. Cosmochimica. Acta* **63**, 3121–3131.

Stipp S. L. S. and Hochella, Jr., M. F. (1991) Structure and bonding environments at the calcite surface as observed with X-ray photoelectron spectroscopy (XPS) and low energy electron diffraction (LEED). *Geochim. Cosmochim. Acta* **55**, 1723–1736.

Stipp S. L. S., Parks G. A., Norstrom D. K. and Leckie J. O. (1993) Solubility-product constant and thermodynamic properties for synthetic otavite, $CdCO_{3(s)}$, and aqueous association constants

for the Cd(II)-CO_2-H_2O system. *Geochim. Cosmochim. Acta* **57**, 2699–2713.

Stipp S. L. S., Eggleston C. M. and Nielsen B. S. (1994) Calcite surface structure observed at microtopographic and molecular scales with atomic force microscopy (AFM). *Geochim. Cosmochim. Acta* **58**, 3023–3033.

Sverjensky D. A. (1984) Prediction of Gibbs free energies of calcite-type carbonates and the equilibrium distribution of trace elements between carbonates and aqueous solutions. *Geochim. Cosmochim. Acta* **48**, 1127–1134.

Sverjensky D. A. (1985) The distribution of divalent trace elements between sulfides, oxides, silicates and hydrothermal solutions: I. Thermodynamic basis. *Geochim. Cosmochim. Acta* **49**, 853–864.

Takasaki S., Parsiegla K. I. and Katz J. L. (1994) Calcite growth and the inhibiting effect of iron (III). *J. Crystal Growth* **143**, 261–268.

Tesoriero A. and Pankow J. (1996) Solid solution partitioning of Sr^{2+}, Ba^{2+}, and Cd^{2+} to calcite. *Geochim. Cosmochim. Acta* **60**, 1053–1063.

Trainor A. and Bartlett B. E. (1961) A possible mechanism of crystal growth from the melt and its application to the problem of anomalous segregation at crystal facets. *Solid-State Electronics* **2**, 106–114.

Van Cappellen P., Charlet L., Stumm W. and Wersin P. (1993) A surface complexation model of the carbonate mineral – aqueous solution surface. *Geochim. Cosmochim. Acta* **57**, 3505–3518.

Wagman D., Evans W. H., Parker V. B., Schumm R. H., Halow I., Bailey S. M., Churney K. L. and Nuttall R. L. (1982) The NBS tables of chemical thermodynamic properties: Selected values for inorganic and C_1 and C_2 organic substances in SI units. *J. Phys. Chem. Ref. Data* **11** (Suppl. 2).

Wang Y. and Xu H. (2001) Prediction of trace metal partitioning between minerals and aqueous solutions: a linear free energy correlation approach. *Geochim. Cosmochim. Acta* **65**, 1529–1543.

Watson E. B. (2004) A conceptual model for near-surface kinetic controls on the trace-element and stable isotope composition of abiogenic calcite crystals. *Geochim. Cosmochim. Acta* **68**, 1473–1488.

Watson E. B. and Liang Y. (1995) A simple model for vector zoning in slowly grown crystals: implications for growth rate and lattice diffusion, with emphasis on accessory minerals in crustal rocks. *Am. Miner.* **80**, 1179–1187.

Zachara J. M., Cowan C. E. and Resch C. T. (1991) Sorption of divalent metals on calcite. *Geochim. Cosmochim. Acta* **55**, 1549–1562.

Zachara J. M., Kittrick J. A. and Harsh J. B. (1988) The mechanism of Zn2+ adsorption on calcite. *Geochim. Cosmochim. Acta* **52**, 2281–2291.

Associate editor: Jacques Schott